Direct numerical simulation of unsteady flow in channel with rough walls

Kiran Bhaganagar[a)]
Department of Mechanical Engineering, University of Maine, Orono, Maine 04468, USA

(Received 31 December 2007; accepted 1 June 2008; published online 31 October 2008)

A fundamental study has been performed to understand the effect of unsteady forcing on turbulence statistics in channel flow with rough walls using direct numerical simulation. Unsteady flows have been generated by applying an unsteady nonzero mean forcing in the form of time varying pressure gradient such that the amplitude of oscillations is between 19% and 26% of mean centerline velocity and covering a range of forcing frequencies. The analysis has revealed unsteady forcing, depending on the forcing frequency, results in enhanced roughness compared to steady channel flow. The rough-wall flow dynamics have been categorized into high-, intermediate-, and low-frequency regimes. In the regime of high-frequency forcing, unsteadiness alters the mean velocity and turbulence intensities only in the inner layer of the turbulent boundary layer. Further, the turbulence intensities are out of phase with each other and also with the external forcing. In the regime of intermediate-frequency forcing, mean velocity and turbulence intensities are altered beyond the inner layer. In the inner layer, the turbulence intensities are out of phase with each other. The Reynolds stress is in phase with the external forcing in the inner layer, but it is out of phase in the outer layer. In the regime of low-frequency forcing, the mean velocity and turbulence intensities are significantly altered throughout the turbulent boundary layer. © *2008 American Institute of Physics*. [DOI: 10.1063/1.3005859]

I. INTRODUCTION

Turbulent flow in channel with rough walls has been studied extensively, yet our current understanding is mostly confined to quasisteady turbulent flows. However, in many real life applications such as physiological flows (blood flow in diseased coronary artery) and coastal flows (flow over rough ocean bed), the flow conditions are either oscillatory (zero mean) or pulsatile (nonzero mean) in nature. The unsteady flow effects over rough surfaces are not well understood and even the fundamental questions have not yet received a satisfactory answer (for example, Ref. 1). In particular, the response of the mean flow and the fluctuating components of turbulence to different forcing frequencies needs to be understood. The presence of surface roughness is as such a complex phenomena and the flow unsteadiness enhances the complexity of the problem. For example, it is known that in a quasisteady flow, the shedding of vortices due to roughness elements occurs at a frequency that depends on the geometrical roughness parameters, and when the external forcing frequency is comparable to this shedding frequency, the interaction of these two phenomena makes the flow physics further complicated.

In quasisteady turbulent flow in a channel with rough surfaces the effects of surface roughness on turbulence statistics has been well studied. In light of the wide range of experimental and numerical results (e.g., Refs. 2–7) it is now clear that roughness alters the inner layer of the turbulent boundary layer, and for some rough surfaces the inner layer communicates with the outer layer thus altering the entire turbulent boundary layer. In the presence of external forcing the nature of these inner/outer layer interactions and their sensitivity to the forcing frequency is still not clear. In particular, classifying the unsteady rough-wall dynamics into regimes based on forcing frequency will be of fundamental importance.

The quasisteady turbulent channel flow over rough walls has been investigated by Bhaganagar *et al.*,[8,9] and Sen *et al.*[10] For this purpose, a highly accurate and well resolved direct numerical simulation (DNS) tool has been developed to simulate flow over a rough wall with three-dimensional (3D) roughness elements arranged in an "egg carton" pattern. The roughness parameters used are analogous to, for example, case 11 of Schlichting's regular roughness patterns.[11] The egg carton roughness used is thus comparable in terms of its effect on the mean velocity to uniformly packed spheres with distance to diameter ratio of 0.46. A detailed study of the mean velocity and turbulence statistics, such as root-mean-square (RMS) of velocity and vorticity fluctuations and Reynolds stress, has shed light on important mechanisms of rough-wall flow dynamics. The results have further revealed that turbulence statistics can be characterized in terms of roughness height (k) and spacing between the roughness elements (l_x, l_z). Based on these results the egg carton pattern qualifies as a good choice to understand the roughness dynamics even for unsteady flow dynamics. Unsteady flow simulations will be performed using the same numerical and physical parameters used for the steady channel flow study. Important fundamental questions that arise, which will be addressed in this paper: (1) Are the long-time averaged turbulent statistics altered due to unsteady effects? (2) Are the inner and the outer layers of the turbulent boundary layer (TBL) in a channel modified due to external forcing of the mean flow? (3) How are the large-scale features as repre-

[a)]Electronic mail: kiran.bhaganagar@maine.edu.

sented by the RMS of velocity fluctuations altered compared to steady flow? The present study will enhance our current understanding of unsteady flow dynamics in a channel with rough walls.

In order to characterize the unsteady flow over rough walls, it is important to establish physically relevant similarity parameters by identifying the scales that are introduced due to unsteadiness. A relevant length scale for unsteady flows is generally the thickness of the oscillating boundary layer, $l_s=\frac{2\nu}{\omega}$, where ν is the kinematic viscosity and ω is the frequency of oscillation, which is obtained from a trivial extension of the Stokes second problem (for example, Refs. 12–15). Based on l_s, a similarity parameter that was independently introduced by Ronneberger and Ahrens[12] and by Binder and Kueny[16,17] is the viscous Stokes length, $l_s^+=(l_s u_\tau/\nu)$, where u_τ is the wall-friction velocity. It should be noted that the forcing frequency scaled in inner variables can also be directly expressed in terms of l_s^+ as $\omega^+=[2/(l_s^+)^2]$. It has been observed that for high enough forcing frequency, such that $l_s^+<12$, the oscillating flow near the wall follows closely the viscous Stokes solution. For this high-frequency forcing as the oscillatory boundary layer is confined within the viscous layer of the turbulent boundary layer, i.e., up to $y^+=12$, the turbulent flow is dominated only by viscous effects, and turbulence does not play a major role in momentum transport, viscosity alone diffuses the wall-shear stress. This flow can be classified as high-frequency regime. For lower frequency forcing l_s^+ extends beyond the viscous layer of the turbulent boundary layer and a departure from the viscous Stokes behavior is observed. Turbulence, in addition to viscosity, will transport the momentum. Another additional length scale that is introduced due to unsteadiness is the amplitude of forcing. A similarity parameter that is physically relevant is the ratio of oscillating to mean centerline velocity (a_{uc}). When $a_{uc}<1$, the flow is current dominated. This case is prevalent both in the ocean as well as in physiological flows.

In the past, turbulence models such as Reynolds-averaged Navier–Stokes equations (e.g., Refs. 18 and 19) large-eddy simulations (e.g., Refs. 20–27) have been used to simulate flow over rough surfaces such as ripples and bed forms. Experiments of turbulent oscillatory flow over rough beds were performed by various groups (e.g., Refs. 28–32). The results of these simulations and experiments clearly suggest a need for more detailed analysis of accurate turbulence statistics. To obtain accurate flow physics numerically it is essential to perform simulations without *a priori* assumptions regarding the effect of roughness. DNS tool is a ideal choice toward this direction.

The purpose of the present paper is to investigate unsteady flow in channel with rough walls using DNS. The flow is characterized into different regimes (high, intermediate, and low frequency) based on l_s^+. The amplitude ratio is fixed in the range of $a_{uc}=0.19-0.26$.

This paper is arranged as follows: Sec. II A deals with a brief explanation of the governing equations. Section II B explains the spatial and temporal discretizations used for solving the Navier–Stokes equations. Section II C discusses the details of the immersed body method used to introduce surface roughness. The time varying forcing required to generate the unsteady flow is discussed in Sec. II D. For the purpose of analysis, the pulsatile flow is decomposed using the classical triple decomposition, the details are presented in Sec. II E. The computation of u_τ is presented in Sec. II F. It should be noted that this decomposition is a part of postprocessing analysis. The numerical parameters for the simulations and the results are discussed in Sec. III. The conclusions are presented in Sec. IV.

II. NUMERICAL METHODOLOGY: DIRECT NUMERICAL SIMULATION

DNS solver developed by Bhaganagar *et al.*[8,9] to simulate steady flow in channel with rough walls has been modified to introduce the unsteady forcing. The DNS solver developed is an accurate, robust, parallel, numerical tool to simulate turbulent flow over a complex boundary while retaining the simplicity and efficiency of computation in a Cartesian system by solving the governing Navier–Stokes equations exactly without any approximations. The Navier–Stokes equations are solved in the velocity-vorticity formation.[33] The coordinate system is Cartesian system with (x,y,z) being the streamwise, wall-normal, and spanwise coordinates. The corresponding velocity and vorticity components are represented by (u,w,v) and $(\omega_x,\omega_z,\omega_y)$, respectively.

A. Governing equations

The governing equations are expressed in wall-normal velocity-wall-normal vorticity formulation.[33] This particular formulation has the distinct advantage of eliminating the pressure term from the Navier–Stokes equations while requiring the solution of only two governing equations, namely, an evolution equation for the Laplacian of the vertical velocity and an evolution equation for the normal vorticity. It also leads to reduced storage requirements compared to the primitive variable or vorticity-transport formulation. Refer to Bhaganagar *et al.*[34] for details. The wall-normal component of the curl of the Navier–Stokes equations results in an evolution equation for the wall-normal vorticity, ω_z. Application of the Laplace operator to the momentum equation for the wall-normal component of velocity yields an equation for that component through the use of the momentum and the pressure Poisson equations. For Reynolds number Re, the resulting equations are a second order evolution equation for wall-normal vorticity, ω_z, and a fourth-order evolution equation for wall-normal velocity, w, as follows:

$$\frac{\partial \omega_z}{\partial t} = H_\omega + \frac{1}{\mathrm{Re}}\nabla^2 \omega_z, \tag{1}$$

$$\frac{\partial \nabla^2 w}{\partial t} = H_v + \frac{1}{\mathrm{Re}}\nabla^4 w, \tag{2}$$

$$w(\pm 1) = \frac{\partial w}{\partial y}(\pm 1) = 0, \tag{3}$$

$$\omega_z(\pm 1) = 0, \tag{4}$$

where

$$H_v = -\frac{\partial}{\partial y}\left[\frac{\partial H_1}{\partial x} + \frac{\partial H_2}{\partial z}\right] + \left[\frac{\partial^2}{\partial x^2} + \frac{\partial^2}{\partial z^2}\right]H_3, \tag{5}$$

$$H_\omega = \left[\frac{\partial H_3}{\partial x} + \frac{\partial H_1}{\partial z}\right], \tag{6}$$

$$H = (H_1, H_2, H_3) = u \times \omega, \quad \Delta = \left[\frac{\partial^2}{\partial x^2} + \frac{\partial^2}{\partial z^2} + \frac{\partial^2}{\partial y^2}\right]. \tag{7}$$

It is computationally efficient to split the fourth-order equation for w into two second-order equations and solve the resulting system. For numerical simplicity the fourth-order wall-normal velocity equation [Eq. (2)] is split into two second-order equations as follows:

$$\frac{\partial \phi}{\partial t} = H_v + \frac{1}{\mathrm{Re}}\nabla^4 w, \tag{8}$$

$$\nabla^2 w = \phi. \tag{9}$$

Equation (8) is the evolution equation for the Laplacian of the wall-normal velocity ϕ and Eq. (9) is the Poisson equation for the Laplacian of w. Once the normal velocity and normal vorticity are computed, the other components of velocity are solved by using the continuity constraint and the definition of normal vorticity.

1. Mean flow equations

The equations for the mean flow are obtained by setting the horizontal space derivatives to zero in the Navier–Stokes equations, thus the resulting equations for the mean flow $\mathbf{U} = (U, 0, V)$ are

$$\frac{\partial U}{\partial t} = -P_x + H_1 + \frac{1}{\mathrm{Re}}\nabla^2 U + f_1, \tag{10}$$

$$\frac{\partial V}{\partial t} = H_3 + \frac{1}{\mathrm{Re}}\nabla^2 V + f_3, \tag{11}$$

where P_x is the time varying pressure gradient in the horizontal direction. Refer to Sec. II D for details of P_x to the imposed in order to obtain the desired mean velocity. f_1 and f_3 are the x (streamwise) and z (spanwise) components of the body force terms due to the immersed body as explained in Sec. II C. H_1 and H_3 are nonlinear terms [Eq. (7)].

B. Spatial discretization and temporal integration

In the horizontal $x-z$ directions the spatial discretization is performed using Fourier series expansion assuming periodicity as the flow is statistically homogeneous. In the wall-normal direction, z, the flow is inhomogeneous, and it needs to be well resolved. Hence, high resolution compact finite differences is used to obtain the spatial derivatives $\left(\frac{\partial}{\partial y}\right)$. For typical finite-difference scheme, the low-wave-number components are well resolved but resolving high-wave-number components is difficult due to a large truncation error. Therefore, in order to obtain high resolution accuracy, high order finite differences are necessary.[35] Alternatively, without increasing the formal order of accuracy, spectral-like resolution can be achieved to compute the spatial derivatives using compact finite differences (for details see Ref. 36). Further, they have an added advantage of being computationally efficient as the implementation results in a linear system of equations that can be solved using a tridiagonal solver.

To avoid stringent time-step restrictions, a semi-implicit time integration scheme is implemented to integrate the resultant discretized equations. For the nonlinear terms, an explicit, low-storage, three-stage, fourth-order Runge–Kutta scheme[37] is used and for the linear viscous terms, an implicit Crank–Nicholson scheme is used. The solution at the end of each time step is the sum of the solution of the explicit part and the implicit part. Refer to Carpenter and Kennedy[38] for the details of the formulation.

C. Immersed body method

Immersed body method has been successfully applied in DNS for complex boundary such as wavy surfaces by various groups (for example, Refs. 39–42). The virtual roughness is prescribed within the channel via a body force term, using the immersed body method, by enforcing the no-slip condition at this virtual body.[43] 3D roughness elements are introduced with an egg carton shaped surface $\sigma(x,z)$ such that

$$\sigma(x,z) = \sigma_0 + \frac{1}{4}h\left\{-1 + \left[1 + \sin\left(\frac{2\pi x}{lx} + \frac{2\pi z}{lz}\right)\right] \times \left[1 + \sin\left(\frac{2\pi x}{lx} - \frac{2\pi z}{lz}\right)\right]\right\}, \tag{12}$$

where $\sigma(x,z)$ is measured with respect to the channel coordinates in units of δ (channel half height), h is the (peak-to-valley) roughness height, σ_0 defines the mean offset of the immersed body, and l_x and l_z are the streamwise and spanwise wavelengths (peak-to-peak distance) of the roughness elements. We chose $\sigma = -0.96$ for all simulations presented here, which prescribes the virtual no-slip roughness surface at the bottom of the DNS domain, just above the lower wall. For this surface, the roughness "bumps" extend $3h/4$ above σ_0, while the valleys lie $h/4$ below it.

The definition of the body force term is described as follows: A first-order temporal discretization of the Navier–Stokes equations is employed,

$$\frac{u^{n+1} - u^n}{\delta t} + u^n \cdot \nabla u^n = -\nabla p^n + \nu \nabla^2 u^n + \mathbf{f}, \tag{13}$$

where $\mathbf{f} = (f_1, f_2, f_3)$ is the body force, $\mathbf{u} = (u, w, v)$ is the velocity vector, p is the pressure, ν is the kinematic viscosity, δt is the time-step increment, and the superscripts n and $n+1$, respectively, indicate the current and next time level. On the immersed body $\sigma(x,z)$, the velocity is zero, such that

$$u^{n+1} = (0,0,0), \tag{14}$$

and the body force is approximated as

$$\mathbf{f} = \frac{\mathbf{V} - \mathbf{u^n}}{\delta \mathbf{t}} + \mathbf{u^n} \cdot \nabla \mathbf{u^n} + \nabla \mathbf{p^n} - \nu \nabla^2 \mathbf{u^n}, \tag{15}$$

where $V=(0,0,0)$.

The time-dependent body force is applied at a set of two points, the one just below the immersed body and the one just above. When the body coincides with the grid, the body force is applied at the body and at a point below. This method gives flexibility in choosing the immersed body not found in some other methods, since there is no need to line up the body with a grid.

D. Unsteady forcing

This section explains the details of obtaining the time varying pressure gradient that needs to be imposed in order to obtain desired mean flow.

A horizontal pressure gradient is imposed such that the desired mean velocity (U) composed of a nonzero steady component $(\bar{U})$ and an oscillatory component $(\tilde{U})$ is generated. If we desire an oscillatory component to be of the form: $\tilde{U}(y,t)=U_m(y)\sin[(2\pi/T)t]$, where U_m is the wave-induced amplitude, $\omega=2\pi/T$ is the wave frequency, and T is the wave period. As the mean flow satisfies the mean momentum equation, the required pressure gradient is obtained from the mean momentum equation [see Eq. (10)] as

$$\frac{\partial U}{\partial t} = -\frac{dP_o}{dx} + \frac{1}{\mathrm{Re}}\frac{\partial^2 U}{\partial y^2} + f_1, \tag{16}$$

where dP_o/dx is the mean pressure gradient that is imposed, f_1 is the streamwise (x) component of the body force generated by the immersed body. Integrating the above equation from the lower wall to the upper wall of the channel yields

$$\int_{-1}^{1} \omega U_m \sin(\omega t) dy = -\int_{-1}^{1} \frac{dP_o}{dx} dy + \int_{-1}^{1} \frac{1}{\mathrm{Re}}\frac{\partial^2 U}{\partial y^2} dy + \int_{-1}^{1} f_1 dy. \tag{17}$$

The required pressure gradient to obtain the desired form of the mean velocity is obtained as

$$\frac{dP_o}{dx} = -U_m \omega \sin(\omega t) + \frac{1}{2\,\mathrm{Re}}\left(\left.\frac{dU}{dy}\right|_{y=+1} - \left.\frac{dU}{dy}\right|_{y=-1} \right) + \int_{-1}^{1} f_1 dy. \tag{18}$$

The last term is evaluated by using the standard trapezoidal integration method for nonuniform mesh. The time varying pressure gradient is computed at the end of each Runge–Kutta substep.

E. Decomposition of pulsatile flows

As a part of postprocessing analysis of the DNS data, the resultant DNS flow fields are decomposed using the classical decomposition for oscillatory flows (e.g., Ref. 44). The quantity f is decomposed into a phase-averaged mean component $(\langle f \rangle)$ and a fluctuating component (f') of f that represents the deviation from the mean. The phase-averaged mean component can be represented by a long-time mean $(\bar{f})$ and a periodic, oscillatory component $(\tilde{f})$ of f as follows:

$$f(y,t) = \langle f(y,t) \rangle + f'(y,t), \tag{19}$$

$$\langle f \rangle (y,t) = \bar{f}(y) + \tilde{f}(y,t). \tag{20}$$

For a domain of size L_x in the streamwise direction, L_z in the spanwise direction, for an oscillation of time period T, the long-time mean is defined as

$$\bar{f}(y) = \frac{1}{TL_xL_z}\int_0^T \int_0^{L_x} \int_0^{L_z} f(x,y,z,t) dx dz dt \tag{21}$$

and the phase-averaged quantity is defined as

$$\langle f \rangle (y,t) = \frac{1}{L_xL_z}\int_0^{L_x} \int_0^{L_z} f(x,y,z,t) dx dz. \tag{22}$$

It is often convenient to express the periodic oscillatory component by the amplitudes and phases of the successive terms of the Fourier series as

$$\tilde{f}(y,t) = \sum_{n=1}^{\infty} A_{\tilde{f}}^n(y) \sin[n\omega t + \phi_{\tilde{f}}^n(y)], \tag{23}$$

where $A_{\tilde{f}}^n$ is the amplitude and $\phi_{\tilde{f}}^n$ is the phase for mode n of the oscillating component of quantity f. It has been generally observed that the fundamental mode is dominant and higher modes are less substantial. It is accurate to represent the oscillatory component of f by the amplitude and the phase of the fundamental, i.e., $A_{\tilde{f}}^1$ and $\phi_{\tilde{f}}^1$. An added advantage of this representation: the accurate physics and correct representation of time varying functions is still retained and at the same time it is not necessary to use the full representation of all these time functions which can be extremely cumbersome.

For the sake of convenience, the amplitude and the phase of the fundamental mode will be presented without a superscript, i.e., as $A_{\tilde{f}}$ and $\phi_{\tilde{f}}$. As an example, according to this notation, the amplitude and phase of the fundamental mode $A_{\tilde{U}}$, $\phi_{\tilde{U}}$ represent the oscillatory component of mean velocity.

F. Computation of u_τ

The wall-shear velocity (friction velocity), u_τ is obtained by solving the x (streamwise) momentum equation for the mean velocity,

$$0 = -\frac{\partial p}{\partial x} + \frac{1}{\mathrm{Re}}\Delta U + f_1, \tag{24}$$

where f_1 is the x component of the body force term $\mathbf{f}$ [refer to Eq. (15)]. As the nondimensional domain extends from $y=-1$ to $y=+1$ in the wall-normal direction, integrating the above equation from the lower wall $(y=-1)$ to the upper wall $(y=+1)$ results in the u_τ at the rough surface as follows:

$$u_\tau = -2\frac{dp}{dx} + \frac{1}{\mathrm{Re}}\left.\frac{dU}{dy}\right|_{y=1} + \int_{y=-1}^{y=1} f_1 dy. \tag{25}$$

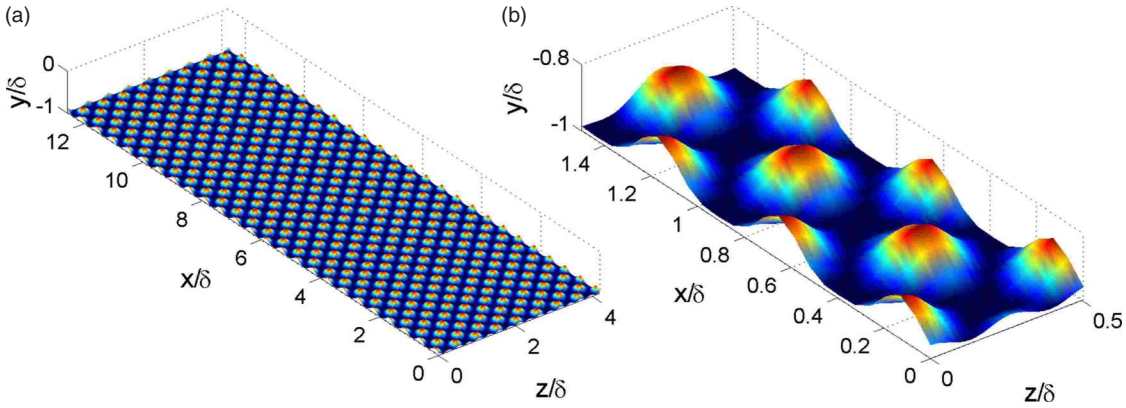

FIG. 1. (Color online) (a) The channel is shown from the lower wall ($y/\delta=-1$) to its centerline ($y/\delta=0$) with roughness surface of $h^+=21.6$. The streamwise and spanwise roughness-element periods are, respectively, $l_x/\delta=4\pi$ and $l_z/\delta=4\pi/3$. (b) A portion of the lower rough wall to highlight the roughness peaks and valleys.

The last term of the above equation is evaluated using a trapezoidal rule for a nonuniform mesh. u_τ is computed at every $x-z$ grid point, and is averaged over all these locations.

III. RESULTS

Flow simulations have been performed for unsteady flows at different flow conditions corresponding to $l_s^+=5,11,24$. The corresponding frequency in wall units is $\omega^+=0.07,\ 0.017,\ 0.0034$, and the time period (scaled by u_τ and δ) is $T=0.5,2,10$. Simulations also have been performed for steady flow over rough wall, which will be referred to as the steady case or steady flow. In all the unsteady simulations pressure gradient has been imposed such that the amplitude of oscillating centerline velocity ($\tilde{U}_c$) is around 19%–26% of long-time mean centerline velocity ($\bar{U}_c$). There is no straightforward relation between the imposed pressure gradient and $(\tilde{U}_c)/(\bar{U}_c)$, hence for each frequency case the simulations had to be performed a few times by adjusting the amplitude of the forcing until the desired value is attained.

DNS has been performed for $\mathrm{Re}_\tau=180$ (Reynolds number based on wall-shear velocity u_τ and channel half height δ) in a periodic channel of streamwise and spanwise sizes $L_x/\delta=4\pi$ and $L_z/\delta=4/3\pi$, where 2δ is the distance between the walls. The spatial discretization uses 194 streamwise Fourier modes, 192 wall-normal compact finite-difference grid points of fourth-order accuracy and 192 spanwise Fourier modes. The roughness elements given by Eq. (12) are specified with peak-to-peak spacing in the streamwise and spanwise directions of 100 wall units and height of $h^+=20$. The roughness surface corresponding to $h^+=20$ and the physical domain is shown in Fig. 1.

The detailed velocity flow fields obtained from the DNS of unsteady flow in a channel with rough walls are analyzed. Once the long-time mean velocity has reached a statistically steady state, the computations were continued in time for an additional 20 time periods to obtain phase-averaged statistics (which were gathered by averaging over the horizontal x and z directions as well as over the 20 time periods). Tests were performed to verify adequate spatial and temporal convergences of the mean statistics.

It should be noted, by definition, long-time average of the mean component and the fluctuating (turbulent) components are functions of the wall-normal direction only. The phase-averaged components are functions of time and wall-normal distance.

A. Mean velocity

For the purpose of analysis, the mean velocity is decomposed using Eqs. (19) and (20). The effect of forcing on the mean velocity can be understood by considering the long-time averaged mean component and the oscillatory component. Using Eq. (21), the long-time averaged mean velocity ($\bar{U}$) is evaluated for the unsteady cases.

1. Long-time averaged mean velocity

The effects of roughness on statistically averaged mean flow velocity are generally parametrized based on an equivalent sand-grain roughness height (e.g., Ref. 45). The classical framework established by Schlichting[11] predicts the effect of roughness on the mean velocity distribution is confined to a thin wall layer. In the log region, assuming a logarithmic velocity distribution for flow over a smooth wall is given by

$$\frac{U}{u_\tau}=\frac{1}{\kappa}\ln\left(\frac{yu_\tau}{\nu}\right)+C_0, \tag{26}$$

the rough-wall modification is

$$\frac{U}{u_\tau}=\frac{1}{\kappa}\ln\left(\frac{yu_\tau}{\nu}\right)+C_0-\frac{\Delta U}{u_\tau}, \tag{27}$$

where $\Delta U/u_\tau=f(k_s^+)$ is the roughness function, k_s^+ in the roughness function is the equivalent sand-grain roughness, and we assume $\kappa=0.41$, $C_0=5.5$ is the additive constant for both the rough and smooth wall, u_τ is the wall-shear velocity.

In the presence of surface roughness the logarithmic velocity profile becomes a straight line only if the vertical axis is shifted by the virtual offset. In order to represent the mean

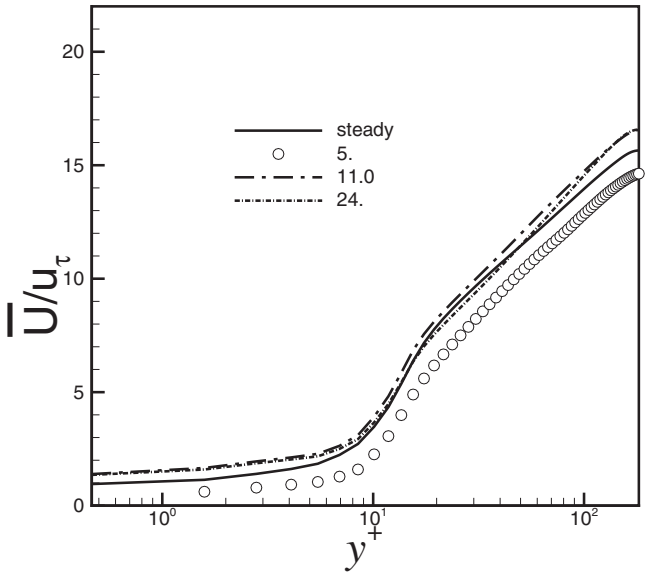

FIG. 2. Long-time average mean velocity scaled by u_τ plotted vs wall-normal distance in wall units for steady case and unsteady cases corresponding to $l_s^+=5,11,24$.

velocity profile over roughness using DNS results, the first task is to determine a virtual offset, α, for the rough wall. The boundary layer over a rough surface is characterized by a surface layer, which can be subdivided into inertial and roughness sublayer.[3] The flow in the inertial sublayer is known to be logarithmic, the mean velocity profile can be described by the common logarithmic law,

$$\frac{U}{u_\tau}=\frac{1}{\kappa}\ln\frac{(y-\alpha)}{y_0}, \tag{28}$$

where y_0 is the roughness length and α is the zero-plane displacement which represents the virtual offset due to roughness. It was shown that α and y_0 are surface properties determined solely by the roughness geometry.[46] They are obtained by fitting the mean velocity measurements in the inertial sublayer to the above equation using u_τ as the slope.[46] The roughness height y_0 can be explicitly related to ΔU^+ as shown in Eq. (28).

As shown by Bhaganagar *et al.*[8] for the steady rough-wall channel flow, this roughness configuration results in an expected downward shift of the logarithmic profile relative to the smooth wall corresponding to $\Delta U^+=6.14$, and with no discernible change in slope. It corresponds to an equivalent sand-grain roughness of $k_s^+=48$; that the ratio of k_s to the physical peak-to-valley height h is thus 2.2. This k_s/h value is analogous to, for example, case 11 of Schlichting's regular roughness patterns.[11] The egg carton roughness used here is thus comparable in terms of its effect on the mean velocity to uniformly packed spheres, with distance to diameter ratio of 0.46. Here, a similar analysis is performed for the three unsteady cases and the effect of forcing frequency on apparent roughness is investigated.

TABLE II. For the three different cases the orbital amplitude scaled in wall units, ratio of the orbital amplitude to the sand-grain roughness.

Case	a^+	a^+/k_s^+	Class of frequency
1	115	2.0	High
2	470	11.5	Intermediate
3	2400	50	Low

Figure 2 shows the distribution of $\bar{U}$ scaled by corresponding u_τ for the unsteady conditions. Also shown in the figure is the statistically averaged mean for steady flow. The unsteady simulations presented are for $l_s^+=5,11,24$. The friction or shear velocity u_τ has been obtained by solving the momentum equations at the wall. The magnitude of u_τ for all the cases is shown in Table I. Scaled in this manner the mean velocity profile for the low-frequency forcing ($l_s^+=24$) collapses on the log profile for the steady flow, thus demonstrating that the downward shift of the logarithmic profile and the equivalent sand-grain roughness is similar to the steady case with $\Delta U^+=6.44$ and $k_s^+=48$. For the intermediate-forcing frequency ($l_s^+=11$) the corresponding $\Delta U^+=6.24$ and $k_s^+=41$, which is not a considerable deviation from the steady flow. Whereas, for the high-frequency forcing ($l_s^+=5$) the mean velocity deviates from the steady flow significantly with $\Delta U^+=8.0$ and $k_s^+=56$. The low and intermediate forcings do not alter the apparent roughness and the mean velocity profile can be well represented by the steady channel flow, on the other hand, the high-frequency forcing increases the apparent roughness. To shed light on the flow physics, the amplitude of the orbital motion in wall units defined as $a^+=(U_o^+/\omega^+)$ has been computed for the three cases, as shown in Table II. It varies from 115 to 2400 for the high- to low-frequency forcing cases. The frequency of the vortices shed from the roughness elements is dictated by the spacing between these roughness elements, which is 100 wall units. It is of the same order of magnitude as the amplitude of orbital motion for the high-frequency forcing. This suggests a pos-

TABLE I. Flow conditions for several imposed frequencies. Stokes length scaled in wall units (l_s^+), forcing frequency scaled in wall units (ω^+), time period of oscillation scaled in outer units (T), the ratio of the amplitude of the oscillating centerline velocity to the long-time mean centerline velocity, peak magnitude in a wave cycle of wall shear or friction velocity (u_τ) for the three unsteady cases and the steady case.

Case	l_s^+	ω^+	T	$A_{\bar{U}_c}/\bar{U}_c$	Peak u_τ	Class of frequency
1	5.0	0.07	0.5	0.23	1.94	High
2	11.0	0.017	2.0	0.20	2.27	Intermediate
3	24.0	0.0034	10.0	0.26	1.7	Low
Steady	⋯	⋯	⋯	⋯	1.5	⋯

sibility of resonance between the unsteady forcing and the vortices shed by the roughness elements, resulting in drastic alteration of the mean velocity for the high-frequency forcing compared to the intermediate- and the low-frequency forcing. A similar resonance phenomena was observed by Bandyopadhyay[47] for turbulent flow over a grooved surface. He has demonstrated that grooved cavity flow resonates when the depths of the cavity and the Stokes layer are nearly the same. For this egg carton roughness elements the roughness vortex shedding frequency is characterized by the spacing between the roughness elements, hence when the forcing frequency is of the same order as the roughness spacing, it results in an enhanced roughness which can be attributed to a resonance type of behavior.

In order to further interpret the results, a dimensionless, roughness parameter based on the ratio of the orbital amplitude to the equivalent sand-grain roughness is computed, as shown in Table II. It is seen that a^+/k_s^+ ranges from 1.28 to 50 for high- to low-forcing frequency. It is interesting that the ratio of k_s to the physical peak-to-valley height h is 2.2 for steady flow, and it is comparable to a^+/k_s^+ for the high-frequency forcing. Hence, under resonant conditions the forcing frequency can be expressed in terms of the equivalent sand-grain roughness.

2. Inner and outer layers: Oscillating component of mean flow

In order to understand how the unsteady effects alter the inner and the outer layer of the turbulent boundary layer in a channel flow, the oscillating component of the mean velocity $(\tilde{U})$ is examined. The amplitude $(A_{\tilde{U}})$ and the phase $(\phi_{\tilde{U}})$ of the fundamental mode of $\tilde{U}$ are obtained using Eqs. (21) and (22). Figure 3(a) shows the amplitude of the fundamental mode normalized by the amplitude at the centerline $(A_{\tilde{U}_c})$. For the high-frequency forcing, i.e., $l_s^+=5$, velocity offshoot is observed close to the wall. For the intermediate-frequency forcing, i.e., $l_s^+=11$, velocity offshoot is still present; however, the peak in mean velocity shifts from the inner to the outer layer. For the low-frequency forcing, i.e., $l_s^+=24$, the peak in mean velocity occurs at the centerline, thus resulting in a thicker profile of the oscillatory boundary layer for lower frequency forcing compared to intermediate- or high-frequency cases. This trend of the variation of the boundary layer thickness with forcing frequency appears to be consistent with the results of Sleath[28] and Jonsson.[48]

Figure 3(b) shows the phase shift relative to the mean centerline velocity. For the high-frequency forcing, i.e., $l_s^+=5$, the mean flow lags behind the centerline velocity in the inner layer. Away from the wall the mean flow moves with the same phase and amplitude as the centerline velocity. Thus, the flow in the outer layer resembles a uniformly enhanced flow. For the intermediate-frequency forcing, i.e., $l_s^+=11$, a phase lead is observed up to $y^+=100$, beyond which the mean flow has the same phase as the mean centerline velocity. For the low-frequency forcing, i.e., $l_s^+=24$, there is significant phase difference of the mean flow relative to the centerline velocity throughout the boundary layer. Near the wall $(y^+=0)$ a phase lead of the mean velocity relative to the centerline velocity is present, however, no particular monotonic trend with the frequency is observed.

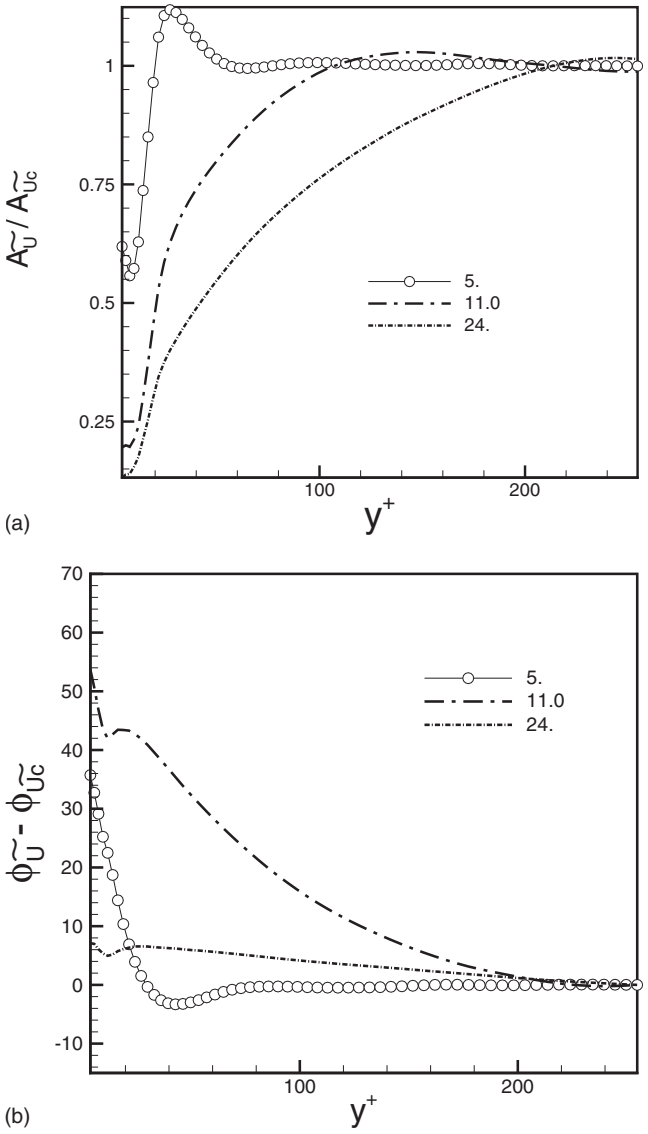

FIG. 3. The oscillatory component of the mean velocity for unsteady cases corresponding to $l_s^+=5$, 11, 24. (a) Amplitude profile of the fundamental mode scaled by the amplitude at the centerline. (b) Phase shift profiles with respect to the centerline plotted vs wall-normal distance in wall units.

B. RMS of velocity fluctuations

The higher order statistics are examined next. The velocity statistics are considered, since its behavior allows us to infer how roughness affects the largest scale features of the flow. The RMS of the velocity fluctuations are decomposed using Eq. (19). Equation (21) is used to obtain the long-time average of turbulence intensities $(\overline{uu},\overline{vv},\overline{ww})$.

Figures 4(a), 5(a), and 6(a) are the long-time averaged RMS of streamwise, wall-normal, and spanwise velocity fluctuations scaled by wall-friction velocity, u_τ, respectively, plotted in wall units. On comparison of the steady and unsteady profiles, it is clear that the RMS profiles for the steady and unsteady cases collapse both in the inner and the outer

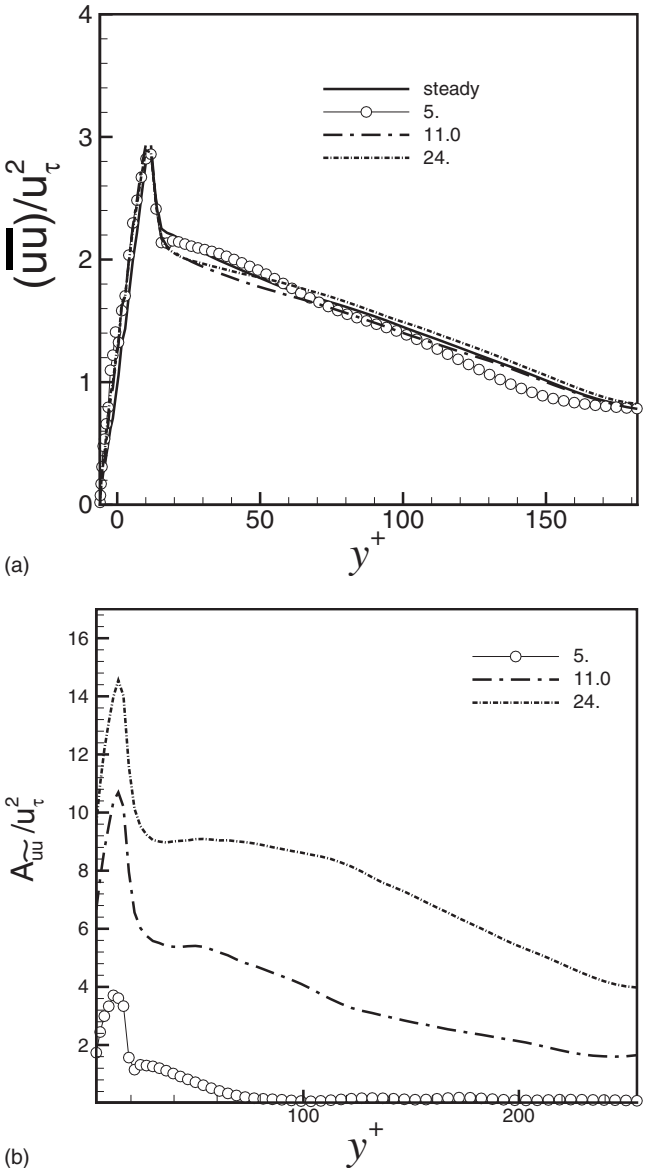

FIG. 4. RMS of the streamwise velocity fluctuations. (a) Long-time averaged component for the unsteady cases ($l_s^+=5$, 11, 24) and the mean component for the steady flow scaled by u_τ plotted in distance from the wall in wall units. (b) Amplitude of the fundamental mode scaled by u_τ plotted vs wall-normal distance in wall units.

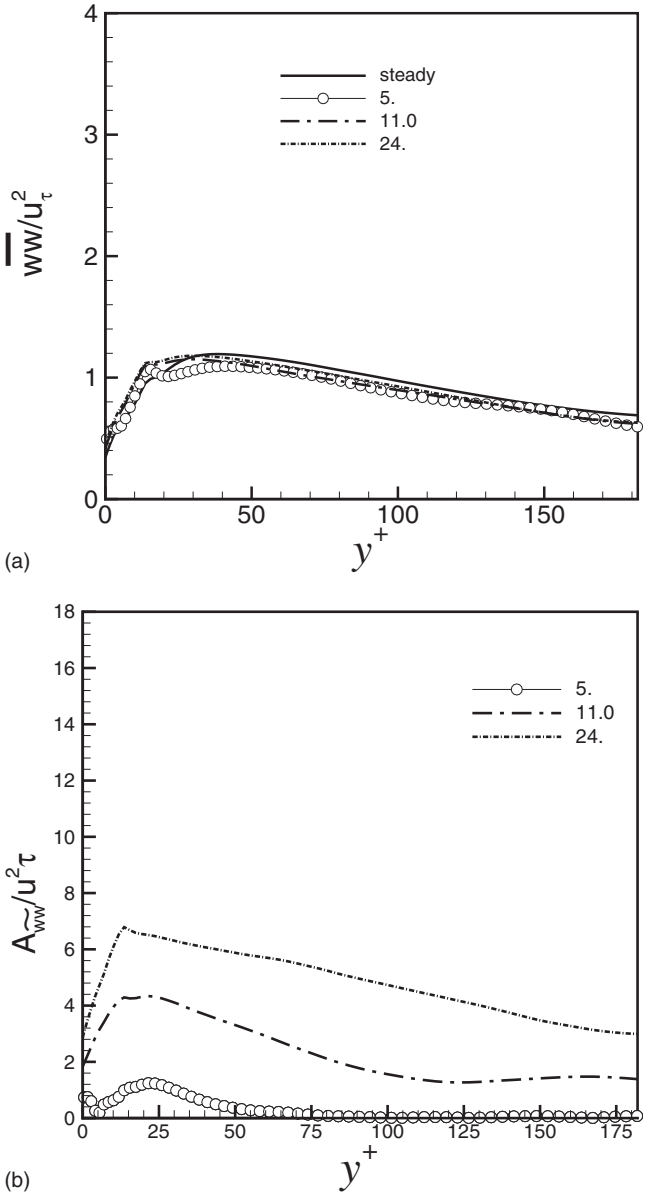

FIG. 5. RMS of the wall-normal velocity fluctuations. (a) Long-time averaged component for the unsteady cases ($l_s^+=5$, 11, 24) and the mean component for the steady flow scaled by u_τ plotted in distance from the wall in wall units. (b) Amplitude of the fundamental mode scaled by u_τ plotted vs wall-normal distance in wall units.

layer of the TBL, thus demonstrating when scaled by u_τ, the long-time averaged RMS of turbulence fluctuations is independent of forcing frequency with no significant deviation from the steady flow.

The oscillating component of the RMS of streamwise velocity fluctuations ($\widetilde{uu}$) as represented by the amplitude of the fundamental wave ($A_{\widetilde{uu}}$) scaled by the corresponding u_τ is shown in Fig. 4(b). In wall units, the location of the peak in RMS of streamwise velocity is independent of forcing frequency, and it is at the same location as for the steady flow. However, the magnitude of this peak depends on the forcing frequency. The corresponding magnitude of $A_{\widetilde{uu}}/u_\tau^2$ for the high-frequency forcing, i.e., $l_s^+=5$ is around 4.0, for the intermediate-frequency forcing, i.e., $l_s^+=11$ is 10.0, respectively, and for the low-frequency case, i.e., $l_s^+=24$ is around 14.0. The following are the important observations from these results: First, the higher the frequency, the smaller the modulation of turbulence is. With increasing forcing frequencies, the modulation of turbulence asymptotes to zero. Second, with increasing frequencies, the modulation tends to zero more rapidly. In the outer layer, for both the high-frequency cases the modulation is close to zero. On the other hand, the modulation for the intermediate and the low-frequency cases are of nontrivial magnitude. At higher frequencies turbulence can no longer follow the imposed forcing and has an attenuated response. It is interesting to note that from the analysis of mean velocity, the high frequency exhibited a resonance type of behavior, but increase in turbulence intensity is not observed. Further work needs to be performed to address this contradiction.

The oscillating components of the wall-normal and the

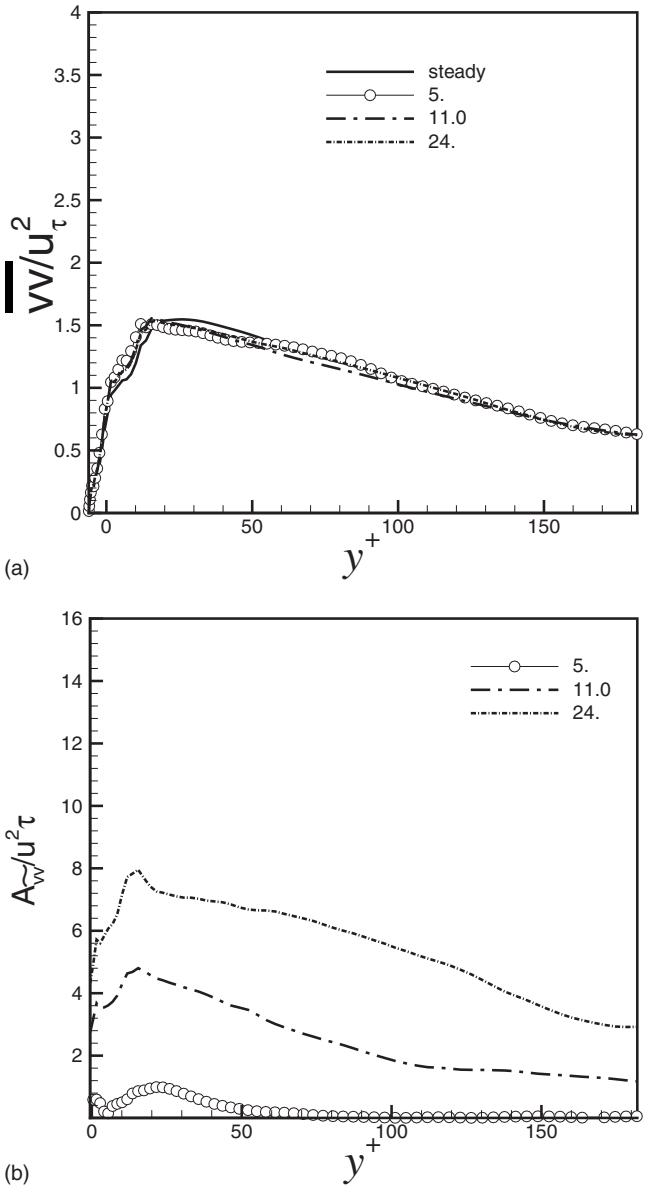

FIG. 6. (a) Long-time averaged component for the unsteady cases ($l_s^+ = 5, 11, 24$) and the mean component for the steady flow scaled by u_τ plotted in distance from the wall in wall units. (b) Amplitude of the fundamental mode scaled by u_τ plotted vs wall-normal distance in wall units.

spanwise velocity components as represented by their corresponding amplitudes of the fundamental wave scaled by u_τ are presented in Figs. 5(b) and 6(b), respectively. The trend is similar to its streamwise counterpart. In the inner layer the peak in RMS of velocity fluctuations is around the same wall-normal distance irrespective of the forcing frequency. In the outer layer both wall-normal and spanwise RMS fluctuations are close to zero for the high-frequency forcing, and they are of nontrivial values for the low and intermediate forcings.

The velocity fluctuations demonstrate that for the high-frequency forcing only the inner layer is affected due to unsteadiness. For the intermediate-frequency forcing the influence of unsteadiness extends into the outer layer, and for the low-frequency forcing the entire turbulent boundary layer is altered due to unsteadiness. There is no significant deviation from steady flow in the long-time averaged mean, turbulence intensities except under resonant conditions.

C. Phase-averaged statistics

To investigate the detailed evolution of turbulence statistics during the wave cycle the phase-averaged quantities are examined. The phase averages of mean velocity ($\langle U \rangle$), the RMS of streamwise ($\langle uu \rangle$), wall-normal ($\langle ww \rangle$), and spanwise velocity ($\langle vv \rangle$) fluctuations are analyzed for the three different forces ($l_s^+ = 5, 11, 24$). The flow statistics at four different times during a wave-cycle ($t = T, T/4, T/2, 3T/4$) are investigated.

1. High-frequency forcing

The phase-averaged statistics for the high-frequency case corresponding to $l_s^+ = 5$ are presented in Fig. 7. Figure 7(a) shows the phase average of mean velocity scaled by u_τ plotted versus the wall-normal distance at four different times during the wave cycle. The wall-normal distance is scaled in wall units. Also shown in the figure is the mean velocity scaled by u_τ for steady flow. Within the wave cycle, based on the velocity profiles, it can be reasonably identified that the accelerating phase is $t = T/2, 3T/4, T$ and the decelerating phase is $t = T, T/4, T/2$. Figure 7(b) shows the phase average of the RMS of streamwise velocity fluctuations ($\langle uu \rangle$) scaled by u_τ plotted versus wall-normal distance in wall units. Scaled in this manner, significant variations of $\langle uu \rangle$ are observed throughout the wave cycle in the inner layer of the turbulent boundary layer. On the other hand, no significant deviations from the steady flow are observed in the outer layer. The peak of RMS. of streamwise velocity fluctuations occurs during the accelerating phase. In the inner layer the peak in $\langle uu \rangle$ moves toward the wall in the accelerating phase and away from the wall in the decelerating phase. The peak oscillates during the wave cycle: it occurs at $y^+ = 18, 24, 38, 17$ during $t = T, T/4, T/2, 3T/4$, respectively. During the acceleration phase, the peak magnitude is higher compared to that of steady flow, and the magnitude is lower to that of steady flow during the deceleration phase. In the outer layer throughout the wave cycle no discernible differences are observed between the unsteady and the steady flow. It means that the unsteady forcing alters only the inner layer and does not affect the outer layer of the TBL and hence, it is similar to the steady flow throughout the wave cycle.

The phase average of the RMS of wall-normal ($\langle ww \rangle$) and spanwise velocity ($\langle vv \rangle$) fluctuations scaled by u_τ are shown in Figs. 7(c) and 7(d), respectively. Significant differences in $\langle vv \rangle$ and $\langle ww \rangle$ are observed throughout the wave cycle in the inner layer. No deviation from the steady flow is observed in the outer layer. The peak in RMS of the wall-normal and the spanwise velocity fluctuations occurs at $t = 3T/4$, i.e., during the deceleration phase, thus suggesting $\langle vv \rangle$ and $\langle ww \rangle$ are out of phase with respect to $\langle uu \rangle$ and also with respect to the mean centerline velocity.

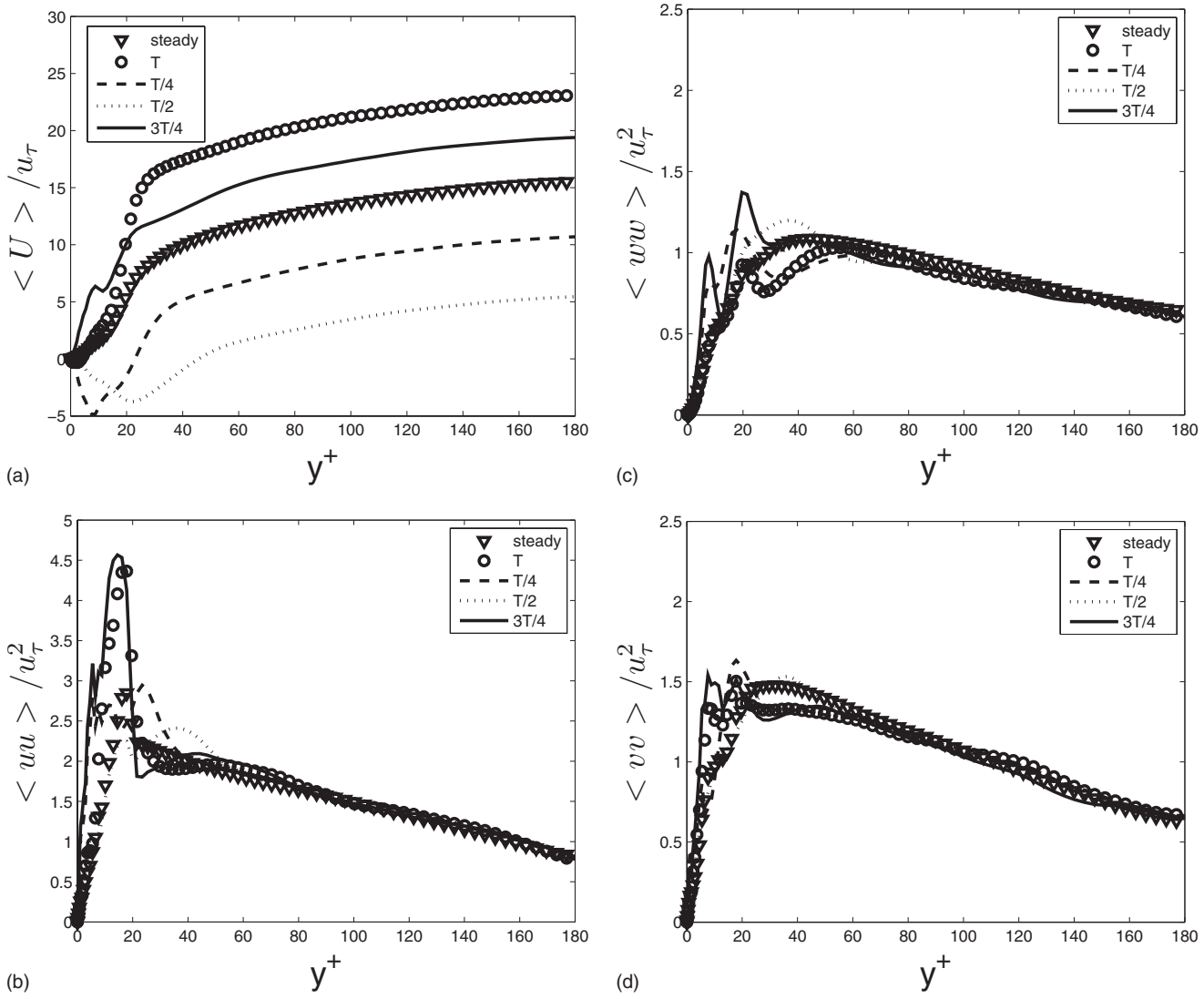

FIG. 7. For $l_s^+=5$ the phase-averaged component at $t=T$, $T/4$, $T/2$, $3T/4$ and the long-time averaged component of the (a) mean velocity, (b) RMS of the streamwise velocity fluctuations, (c) RMS of the wall-normal velocity fluctuations, and (d) RMS of the spanwise velocity fluctuations.

2. Intermediate-frequency forcing

The intermediate-frequency forcing, i.e., $l_s^+=11$, is considered next. Figure 8(a) shows the mean velocity scaled by u_τ at four different times during the wave cycle. It is seen that $t=T$, $T/4$, $T/2$, T is the acceleration phase and $t=3T/4$, T is the deceleration phase. Figure 8(b) shows $\langle uu \rangle$ scaled by u_τ. It is seen that during the deceleration phase, the magnitude of peak in RMS of velocity fluctuations increases and it is closer toward the wall compared to steady flow. During the acceleration phase the magnitude of the peak in RMS of velocity fluctuations decreases and it moves away from the wall. The magnitude and the wall-normal distance of the peak in RMS of velocity fluctuations at $t=T$, $T/4$, $T/2$, $3T/4$ is $y^+=18$, 20, 60, 20 and $\langle uu \rangle / u_\tau=3.5$, 2.0, 2.1, 4.3, 2.8 respectively. For the outer-layer deviation from the steady flow in the RMS profiles are observed throughout the wave cycle. As seen in Figs. 8(c) and 8(d), respectively, the peak in the RMS of both wall-normal and spanwise velocity fluctuations occurs during the deceleration phase, similar to the peak in the RMS of streamwise velocity fluctuations.

3. Low-frequency forcing

The low-frequency forcing, i.e., $l_s^+=24$, is investigated next. Figure 9(a) presents the mean velocity scaled by u_τ at four different times in a wave period. The RMS of streamwise, wall-normal, and spanwise velocity fluctuations are presented in Figs. 9(b)–9(d), respectively. The acceleration phase is $t=T/2$, $3T/4$, T and the decelerating phase is $t=T$, $T/4$, $T/2$. On comparing with steady flow, both the inner and outer layers of $\langle uu \rangle$, $\langle ww \rangle$, and $\langle vv \rangle$ are significantly altered throughout the wave cycle. Further, similar to the previous case, the peak in $\langle uu \rangle$ occurs at the same wall-normal distance throughout the wave cycle, and it is at the same location as for the steady flow. Furthermore, the turbulence intensities are in phase with each other. The peak in

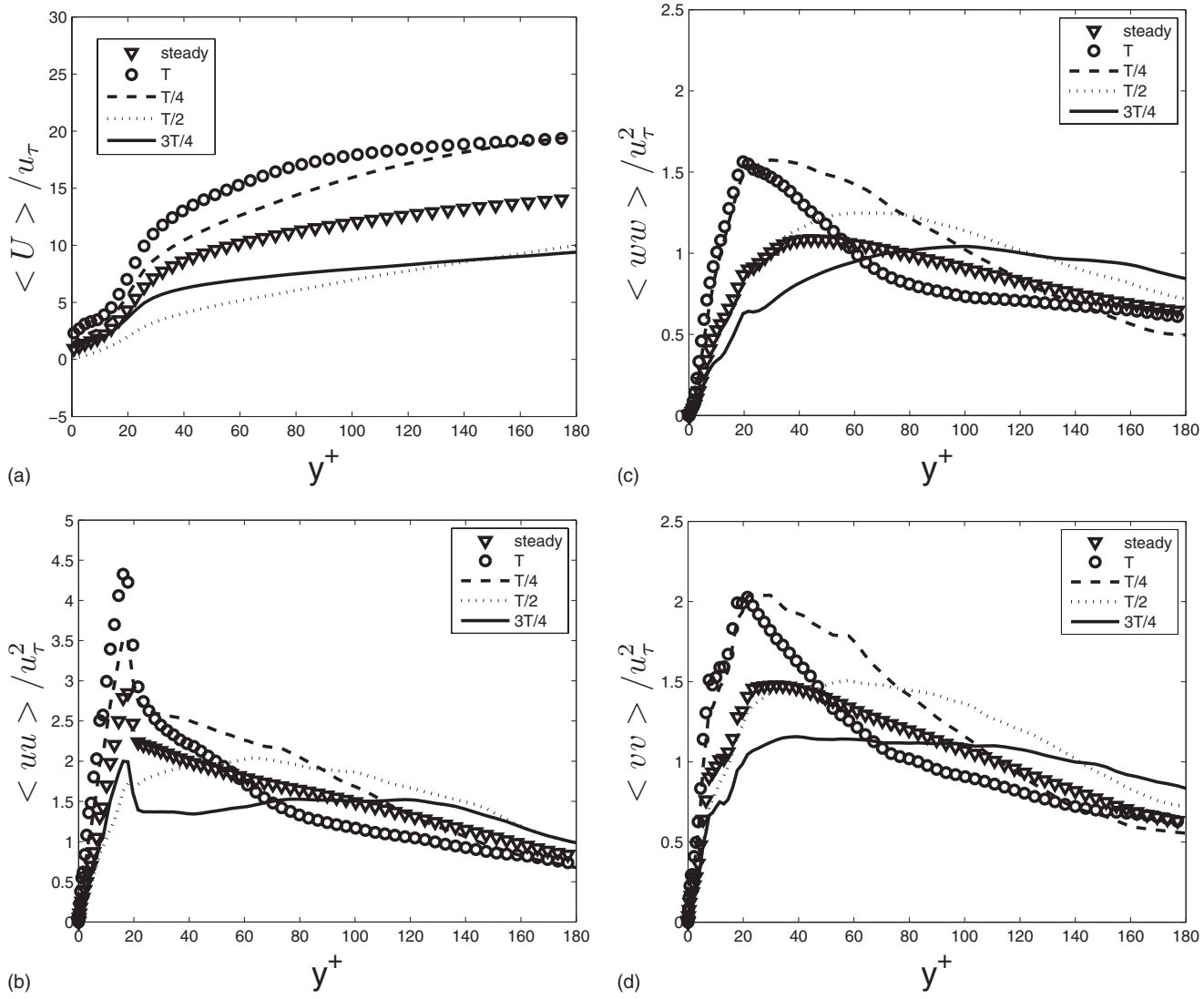

FIG. 8. $t=T$, $T/4$, $T/2$, $3T/4$ and the long-time averaged component of the (a) mean velocity, (b) RMS of the streamwise velocity fluctuations, (c) RMS of the wall-normal velocity fluctuations, and (d) RMS of the spanwise velocity fluctuations.

RMS of velocity fluctuations is altered throughout the cycle: the magnitude of $\langle uu \rangle / u_\tau = 3.4, 1.5, 2.5, 4.0$ at $t = T/4, T/2, 3T/4, T$, respectively. The peak in RMS of the turbulence intensities occurs during the deceleration phase. It is interesting to note that unlike the high and the intermediate frequency, the peak in RMS of velocity fluctuations occurs at the same wall-normal distance throughout the wave cycle as for the steady flow. A similar trend is observed for $\langle ww \rangle$ and $\langle vv \rangle$. The turbulence intensities are in phase with each other.

During the course of the wave cycle significant deviation in the velocity fluctuations from the steady flow is observed. The flow characteristics in inner and outer layers of the TBL can be categorized as high-, intermediate-, and low-frequency regimes.

D. Reynolds stress

Finally, the differences in the time development of Reynolds stress between the high-, intermediate-, and low-frequency regimes are analyzed. Figure 10 shows the phase averages of the Reynolds stress and of the mean centerline velocity at wall-normal distances of $y^+ = 6$, 20, 40, 80. To facilitate a straightforward comparison, the phase averages have been normalized by their peak magnitude during the wave cycle. The phase difference between the Reynolds stress and the external forcing has been determined in the inner and the outer layers of the turbulent boundary layer.

For the high-frequency forcing, as seen in Fig. 10(a), the peak in mean centerline velocity ($\langle U_c \rangle$) occurs around $t/T = 0.5$, whereas the peak in the Reynolds stress at $y^+ = 6$ occurs at $t/T = 0.6$, representing a narrow phase difference with respect to the external forcing. The location of this peak in Reynolds stress changes with wall-normal distance, i.e., for $y^+ = 20$ and 40, the peak shifts to $t/T = 0.7$ and 0.84, respectively, suggesting the phase lead increases with increasing wall-normal distance. This trend is observed in the inner layer. On the other hand, in the outer layer, i.e., at $y^+ = 80$, the Reynolds stress is close to its value for steady channel flow throughout the wave cycle. For the intermediate-frequency forcing, as seen in Fig. 10(b), the peak in $\langle U_c \rangle$ occurs around $t/T = 0.2$. In the inner layer, i.e., at wall-normal distance of

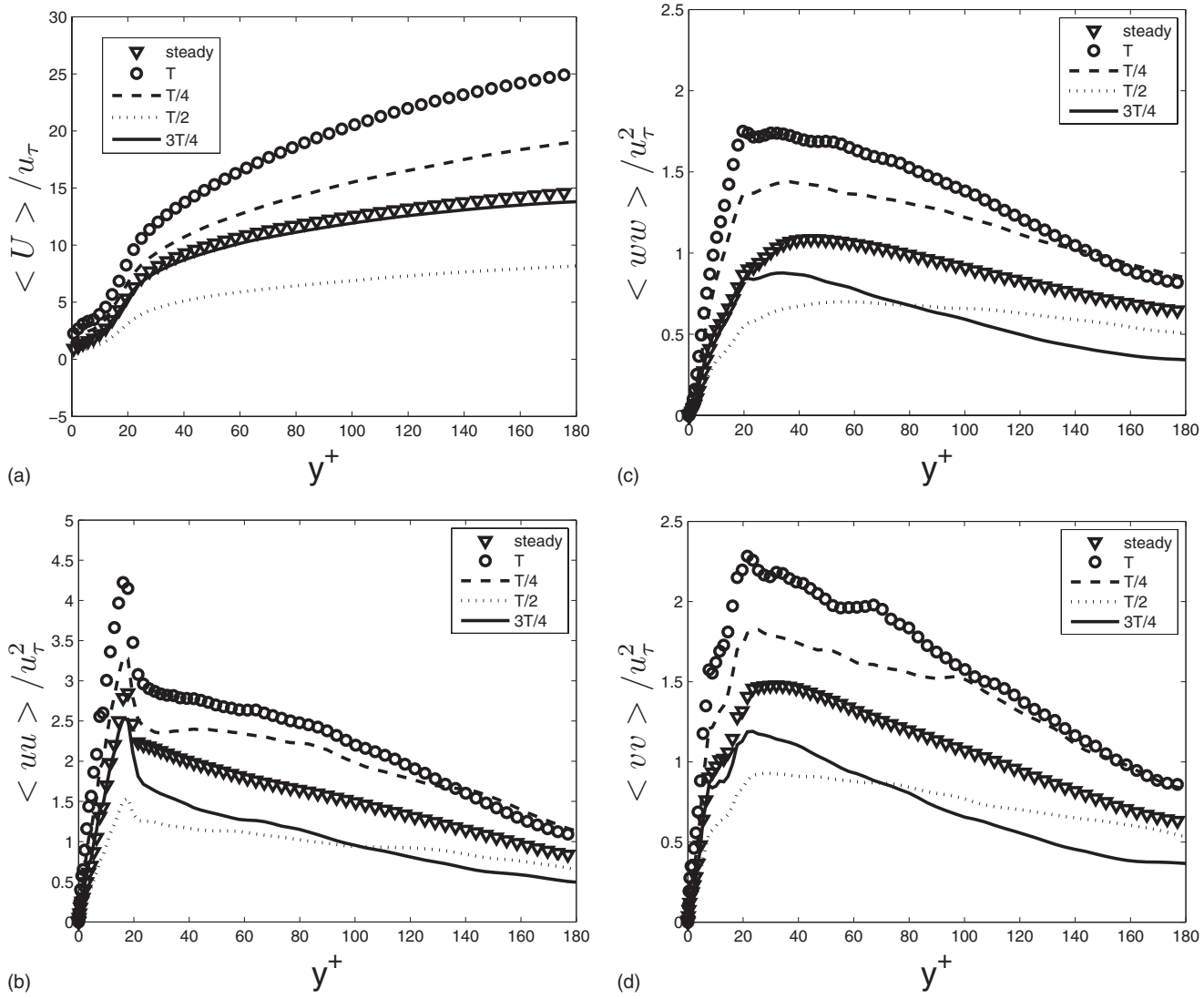

FIG. 9. For $l_s^+=24$ the phase-averaged component at $t=T$, $T/4$, $T/2$, $3T/4$ and the long-time averaged component of the (a) mean velocity, (b) RMS of the streamwise velocity fluctuations, (c) RMS of the wall-normal velocity fluctuations, and (d) RMS of the spanwise velocity fluctuations.

$y^+=6,20$, the Reynolds stress and $\langle U_c \rangle$ are in phase with each other. On the other hand, at $y^+=40$ and 80, the peak in Reynolds stress now occurs at $t/T=0.28$ and 0.4, respectively, a phase difference with respect to the external forcing develops and it increases with increasing y^+. Finally, for the low-frequency forcing, as seen in Fig. 10(c), the Reynolds stress is exactly in phase with $\langle U_c \rangle$. Both in the inner and the outer layers the Reynolds stress is in phase with the imposed forcing. It is also interesting to note that oscillations of the Reynolds stress during the wave cycle are observed not only close to the wall but also even at wall-normal distances further away from the wall. The analysis is consistent with the results of Sleath,[28] who observed that Reynolds stress exhibits different trends in the near-wall region compared to the region away from the wall.

The analysis of turbulence statistics has revealed unsteady flow over rough wall can be characterized into low, intermediate, and high-frequency regimes. The results of this analysis are very critical for developing turbulence models for flow over rough wall, and also for providing closure parameters required for these models. The conclusions are presented in the next section.

IV. CONCLUSIONS

DNS has been used as a tool to simulate pulsatile flow in channel with rough walls. The rough wall consists of 3D roughness arranged in an egg carton pattern. The roughness has been introduced into the physical domain using an elegant immersed body method. The governing equations are the Navier–Stokes equations expressed in the velocity-vorticity formulation. Unsteady flow has been generated by applying an unsteady nonzero mean forcing in the form of time varying pressure gradient such that the amplitude of oscillations is around 19%–26% of the mean centerline velocity. The flow dynamics for low-, intermediate-, and high-frequency forcings have been analyzed to understand the large and small scale features of the flow in the inner and the

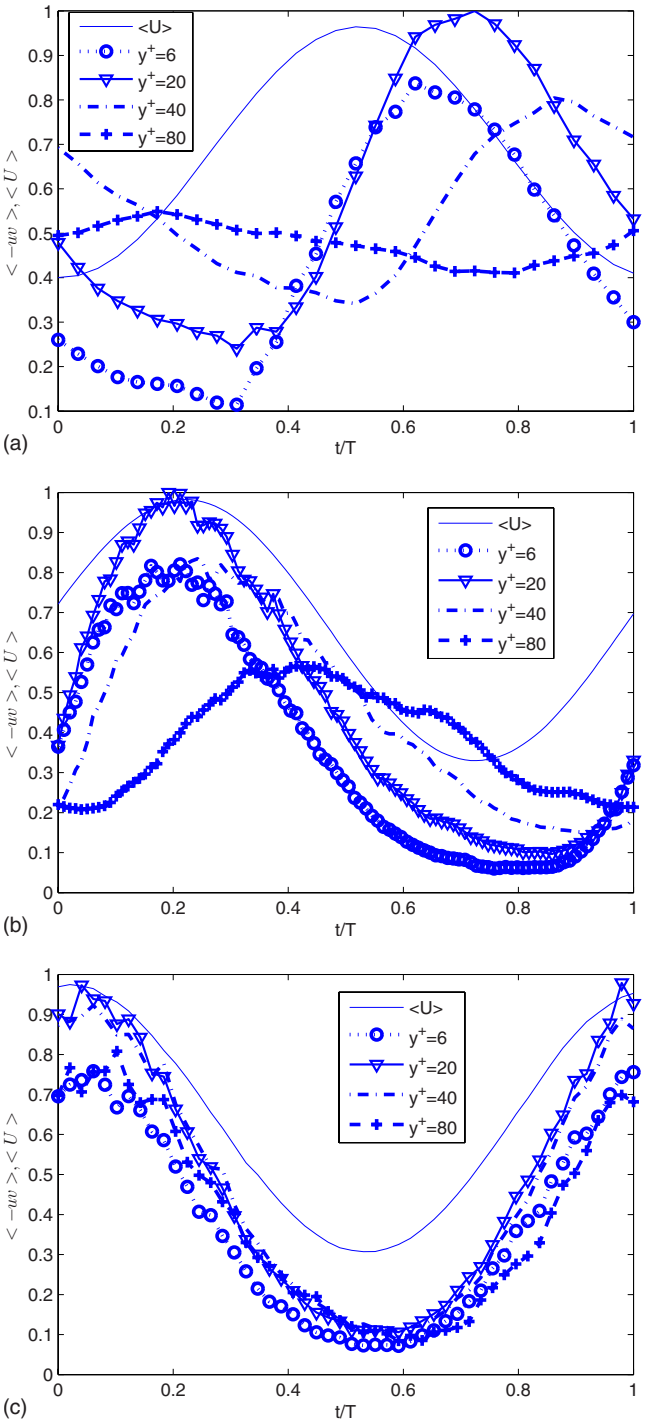

FIG. 10. (Color online) Phase-averaged component of Reynolds stress at wall distance of $y^+=6, 20, 40, 80$. (a) High-frequency case, (b) intermediate-frequency case, and (c) low-frequency case. Also shown in the figure is the phase-averaged mean centerline velocity.

outer layers of the turbulent boundary layer. DNS has been performed for high-frequency forcing of $l_s^+=5$, intermediate-frequency forcing of $l_s^+=11$, and low-frequency forcing of $l_s^+=24$. The simulations have been performed at $\mathrm{Re}_\tau=180$. For the computational mesh, 192 points in the streamwise and spanwise directions and 129 points in the wall-normal direction have been used. For the purpose of analysis, a classical triple decomposition of a flow quantity (q) into long-time average $(\bar{q})$, oscillating component $(\tilde{q})$, and fluctuating component (q') that represents the deviation from the phase-averaged mean has been performed. The phase-averaged mean represents a combination of the long-time average and the oscillating component. The oscillatory component can be well represented by the magnitude and the phase of the fundamental mode.

The rough-wall flow dynamics can be classified into regimes based on forcing frequency as high-, intermediate-, and low-frequency regimes. The effect of the forcing in the inner/outer layers of the turbulent boundary layer can be quantified based on the forcing frequency due to the distinct features exhibited by the rough wall in these regimes.

For the low- and intermediate-frequency forcing the long-time average of the mean velocity is close to that of steady flow. Whereas, for the high-frequency forcing it deviates from the steady flow with an increase in apparent roughness.

The long-time average of the large-scale structures as represented by the RMS of velocity fluctuations is independent of the forcing frequency, and it is close to its value for steady flow. A profound conclusion that can be drawn from the analysis is that the long-time averages of RMS of velocity fluctuations for the unsteady flow can be well represented by the steady channel flow over rough walls.

For the high-frequency forcing, i.e., $l_s^+=5$, the apparent roughness increases compared to the steady flow, and the long-time average of the mean velocity deviates significantly from the steady flow. The change in the apparent roughness is due to the momentum transfer mechanism. The momentum rich, high-speed flow which is brought closer to the rough wall by the turbulence generated by the oscillatory boundary layer, penetrates by turbulent mixing much closer to the rough wall. Thus, leading to an increase in the mean wall-shear stress. The amplitude of the orbital motion in wall units defined as $a^+=(U_o^+/\omega^+)$ varies from 115 to 2400 for the high- to low-frequency forcing cases. The roughness parameter based on the ratio of the orbital amplitude to the equivalent sand-grain roughness ranges from 2 to 50 for high- to the low-frequency forcing. It is interesting that ratio of k_s to the physical peak-to-valley height h is 2.2, and it is comparable to a^+/k_s^+ for the high-frequency forcing. There is a possibility of a resonance type of behavior as the roughness shedding frequency is comparable to the forcing frequency. However, further analysis needs to be performed to validate this hypothesis.

For the high-frequency forcing, the oscillatory boundary layer is confined within the inner layer and the mean velocity has a phase difference with respect to the centerline velocity. The modulation of turbulence decreases with increasing frequency, and it asymptotes to zero modulation for higher frequencies. Also, the modulation of turbulence tends to zero faster with increasing frequencies. All the turbulence intensities are out of phase with each other, and also with Reynolds stress and with $\langle U_c \rangle$. In the outer layer, the mean flow resembles a uniformly enhanced mean flow with negligible modulation of turbulence intensities.

For the intermediate-frequency forcing, i.e., $l_s^+=11.5$, alterations of the mean velocity relative to the steady flow are observed beyond the inner layer. In the inner layer the modu-

lation of turbulence intensities is higher compared to the high-frequency forcing. Furthermore, $\langle uu \rangle$ is in phase with $\langle U_c \rangle$ and with Reynolds stress. However, it is out of phase with $\langle vv \rangle$ and $\langle ww \rangle$. In the outer layer, the mean velocity and the turbulence intensities are enhanced compared to the steady flow. The turbulence intensities are in phase with each other but the Reynolds stress is out of phase with centerline velocity.

For the low-frequency forcing, i.e., $l_s^+ = 24$, the thickness of the oscillatory boundary layer increases compared to the other cases. There is a significant phase difference of the mean velocity with respect to the centerline velocity throughout the boundary layer. The modulation of turbulence intensities is quite substantial throughout the boundary layer. Furthermore, throughout the wave cycle, the turbulence intensities are in phase with each other, and also with both the Reynolds stress and the mean centerline velocity. It is very interesting to note that during the course of the wave cycle, unlike the high- and intermediate-frequency cases, the peak in turbulence intensities is at the same wall-normal distance as for the steady flow.

Surface roughness is a defining feature of flows in natural systems such as environmental flows and physiological flows where flow is essentially turbulent and unsteady. This paper serves as a fundamental study that addresses some of the basic questions regarding the influence of external forcing on the inner and outer layers of the turbulent boundary layer in a channel with rough walls.

ACKNOWLEDGMENTS

This paper is a written version of the presentation by the author at turbulence flow physics workshop conducted at Stanford University, which was held in honor of Professor John Kim on the occasion of his 60th birthday. The author acknowledges the collaborations on rough-wall physics research with Professor Kim.

[1] J. Jimenez, "Turbulent flow over rough walls," Annu. Rev. Fluid Mech. **36**, 173 (2004).
[2] A. E. Perry, K. L. Lim, and S. M. Henbest, "An experimental study of the turbulence structure in smooth- and rough-wall boundary layers," J. Fluid Mech. **177**, 437 (1987).
[3] M. R. Raupach, R. A. Antonia, and S. Rajagopalan, "Rough-wall turbulent boundary layers," Appl. Mech. Rev. **44**, 1 (1991).
[4] P. Krogstad and R. A. Antonia, "Structure of turbulent boundary layers on smooth and rough walls," J. Fluid Mech. **277**, 1 (1994).
[5] C. Lee, "Large-eddy simulation of rough-wall turbulent boundar layers," AIAA J. **40**, 2127 (2002).
[6] P. Orlandi, S. Leonardi, and R. Tuzi, "Direct numerical simulation of turbulent channel flow with wal velocity disturbances," Phys. Fluids **15**, 3587 (2003).
[7] P. Orlandi, S. Leonardi, and R. A. Antonia, "Turbulent channel flow with either transverse or longitudinal roughness elements on one wall source," J. Fluid Mech. **561**, 279 (2006).
[8] K. Bhaganagar, J. Kim, and G. Coleman, "Effect of roughness on wall-bounded turbulence," Flow, Turbul. Combust. **72**, 463 (2004).
[9] K. Bhaganagar, G. Coleman, and J. Kim, "Effect of roughness on pressure statistics," Phys. Fluids **19**, 028103 (2007).
[10] M. Sen, K. Bhagangar, and V. Juttijudata, "Application of proper orthogonal decomposition (POD) to investigate a turbulent boundary layer in a channel with rough walls," J. Turbul. **8**, 19 (2007).
[11] H. Schlichting, *Boundary Layer Theory*. 7th ed. (McGraw-Hill, New York, 1979).
[12] D. Ronneberger and C. D. Ahrens, "Wall shear stress caused by signal amplitude perturbations of turbulent boundary-layer flow: An experimental investigation," J. Fluid Mech. **83**, 433 (1977).
[13] R. Mankbadi and J. Liu, "Near wall response in turbulent shear flows subjected to imposed unsteadiness," J. Fluid Mech. **238**, 55 (1992).
[14] S. Tardu, G. Binder, and R. Blackwelder, "Turbulent channel flow with large-amplitude velocity oscillations," J. Fluid Mech. **267**, 109 (1994).
[15] S. Tardu, "Spectral characteristics of the near-wall turbulence in an unsteady channel flow," Trans. ASME, J. Appl. Mech. **74**, 172 (2007).
[16] G. Binder and J. L. Kueny, "Measurements of the periodic velocity oscillations near the wall in unsteady turbulent channel flow," in *Unsteady Turbulent Shear Flows*, edited by R. Michel and J. Cousteix (Springer-Verlag, New York, 1981), Vol. 100, p. 108.
[17] Z. X. Mao and T. J. Hanratty, "Studies of the wall shear stress in a turbulent pulsating pipe flow," J. Fluid Mech. **170**, 545 (1986).
[18] Y. S. Chang and D. M. Hanes, "Suspended sediment and hydrodynamics above mildly sloped long wave ripples," J. Geophys. Res. **109**, C07022, DOI: 10.1029/2003JC001900 (2004).
[19] J. Fredsoe, K. H. Andersen, and B. M. Sumer, "Wave plus current over a rippled-covered bed," Coastal Eng. **38**, 177 (1999).
[20] D. Henn and R. I. Sykes, "Large-eddy simulation of flow over wavy surfaces," J. Fluid Mech. **383**, 75 (1999).
[21] R. J. Calhoun and R. L. Street, "Turbulent flow over a wavy surface: Neutral case," J. Geophys. Res. **106**, 9277, DOI: 10.1029/2000JC900133 (2001).
[22] Y. S. Chang and A. Scotti, "Modeling unsteady turbulent flows over ripples: Reynolds-averaged Navier–Stokes equations (RANS) versus large-eddy simulation (LES), J. Geophys. Res. **109**, C09012, DOI: 10.1029/2003JC002208 (2004).
[23] B. C. Barr, D. N. Slinn, T. Pierro, and K. B. Winters, "Numerical simulation of turbulent, oscillatory flow over sand ripples," J. Geophys. Res. **109**, C09009, DOI: 10.1029/2002JC001709 (2004).
[24] L. Y. Zou, N. S. Liu, and X. Y. Lu, "An investigation of pulsating turbulent open channel flow by large eddy simulation," Comput. Fluids **35**, 74 (2006).
[25] W. Yue, C.-L. Lin, and V. C. Patel, "Coherent structures in open-channel flows over a fixed dune," J. Fluids Eng. **127**, 858 (2005).
[26] A. Scotti and U. Piomelli, "Numerical simulation of pulsating turbulent channel flow," Phys. Fluids **13**, 1367 (2001).
[27] P. Scandura, G. Vittori, and P. Blondeaux, "Three-dimensional oscillatory flow over steep ripples," J. Fluid Mech. **412**, 355 (2000).
[28] J. F. Sleath, "Turbulent oscillatory flow over rough beds," J. Fluid Mech. **182**, 369 (1987).
[29] R. Macdonald, "Modelling of mean velocity in the urban canopy layer," Boundary-Layer Meteorol. **97**, 25 (2000).
[30] H. M. Nepf and E. R. Vivoni, "Flow structure in depth-limited vegetated flow," J. Geophys. Res. **105**, 28547, DOI: 10.1029/2000JC900145 (2000).
[31] J. Finnigan, "Turbulence in plant canopies," Annu. Rev. Fluid Mech. **32**, 519 (2000).
[32] R. J. Lowe, J. Koseff, and S. Monismith, "Oscillatory flow through submerged canopies: 1. Velocity structure," J. Geophys. Res., [Oceans] **110**, C10016, DOI: 10.1029/2004JC002788 (2005).
[33] P. J. Schmid and D. S. Henningson, *Stability and Transition in Shear Flows*, Springer Series in Applied Mathematical Sciences Vol. 142 (Springer, New York, 2001).
[34] K. Bhaganagar, D. Rempfer, and J. L. Lumley, "Direct numerical simulation of spatial transition to turbulence using fourth-order vertical velocity second-order vertical vorticity formulation," J. Comput. Phys. **180**, 200 (2002).
[35] C. Canuto, M. Y. Hussaini, A. Quarteroni, and T. A. Zang. *Spectral Methods in Fluid Dynamics*, Springer Series in Computational Science and Engineering (Springer-Verlag, New York, 1988).
[36] S. K. Lele, "Compact finite difference schemes with spectral like resolution," J. Comput. Phys. **103**, 16 (1992).
[37] J. H. Williamson, "Low-storage Runge–Kutta schemes," J. Comput. Phys. **35**, 48 (1980).
[38] M. H. Carpenter and C.A. Kennedy, "A fourth order 2N-storage Runge–Kutta scheme," NASA Report No. TM-109112, 1994.
[39] V. De Angelis, P. Lombardi, and S. Banerjee, "Direct numerical simulation of turbulent flow over a wavy wall," Phys. Fluids **9**, 2429 (1997).

[40]P. Cherukat, Y. Na, and T. J. Hanratty, "Direct numerical simulation of a fully developed turbulent flow over a wavy wall," Theor. Comput. Fluid Dyn. **11**, 109 (1998).
[41]Y. Miyake, K. Tsujimoto, and N. Nagai, "Numerical simulation of channel flow with a rib-roughened wall," J. Turbul. **3**, 1 (2002).
[42]P. Orlandi and S. Leanardi, "DNS of turbulent channel flows with two- and three-dimensional roughness," J. Turbul. **7**, 1 (2006).
[43]J. M. Yusof, "Combined immersed-boundary/B-spline methods for simulations of flow in complex geometries," *CTR Annual Research Briefs* (NASA Ames, Stanford University, Stanford, CA, 1997).
[44]G. Brereton and W. Reynolds, "Dynamic response of boundary-layer turbulence to oscillatory shear," Phys. Fluids A **3**, 178 (1991).
[45]W. D. Grant and O. S. Madsen, "Combined wave and current interaction with a rough bottom," J. Geophys. Res. **84**, 1797 (1979).
[46]H. Cheng and I. P. Castro, "Near wall flow over urban-like roughness," Boundary-Layer Meteorol. **104**, 229 (2002).
[47]P. R. Bandyopadhyay, "Resonant flow in small cavities submerged in a boundary layer," Proc. R. Soc. London, Ser. A **420**, 219 (1988).
[48]I. G. Jonsson, "A new approach to oscillatory rough turbulent boundary layers," Ocean Eng. **7**, 109 (1980).